Evolution of superficial lake water temperature profile under diurnal radiative forcing

Nikki Vercauteren,[1,5,6] Hendrik Huwald,[1] Elie Bou-Zeid,[2] John S. Selker,[3] Ulrich Lemmin,[1] Marc B. Parlange,[1] and Ivan Lunati[4]

Received 8 February 2011; revised 18 July 2011; accepted 1 August 2011; published 27 September 2011.

[1] In lentic water bodies, such as lakes, the water temperature near the surface typically increases during the day, and decreases during the night as a consequence of the diurnal radiative forcing (solar and infrared radiation). These temperature variations penetrate vertically into the water, transported mainly by heat conduction enhanced by eddy diffusion, which may vary due to atmospheric conditions, surface wave breaking, and internal dynamics of the water body. These two processes can be described in terms of an effective thermal diffusivity, which can be experimentally estimated. However, the transparency of the water (depending on turbidity) also allows solar radiation to penetrate below the surface into the water body, where it is locally absorbed (either by the water or by the deployed sensors). This process makes the estimation of effective thermal diffusivity from experimental water temperature profiles more difficult. In this study, we analyze water temperature profiles in a lake with the aim of showing that assessment of the role played by radiative forcing is necessary to estimate the effective thermal diffusivity. To this end we investigate diurnal water temperature fluctuations with depth. We try to quantify the effect of locally absorbed radiation and assess the impact of atmospheric conditions (wind speed, net radiation) on the estimation of the thermal diffusivity. The whole analysis is based on the results of fiber optic distributed temperature sensing, which allows unprecedented high spatial resolution measurements (∼4 mm) of the temperature profile in the water and near the water surface.

Citation: Vercauteren, N., H. Huwald, E. Bou-Zeid, J. S. Selker, U. Lemmin, M. B. Parlange, and I. Lunati (2011), Evolution of superficial lake water temperature profile under diurnal radiative forcing, *Water Resour. Res., 47*, W09522, doi:10.1029/2011WR010529.

1. Introduction

[2] Accurate knowledge of temperature at the air–water interface is crucial to understand the transfer of heat, moisture, and momentum between the atmosphere and an underlying water surface. Specifically, understanding the heat storage in water bodies is essential to estimate evaporation by means of the widely used energy budget methods [e.g., *Brutsaert*, 2005; *Katul and Parlange*, 1992; *Penman*, 1948; *Priestley and Taylor*, 1972]. Moreover, the turbulent aspect of the energy transfers makes it important to understand the dynamics of the temperature distribution within the water column.

[3] However, observations of the transfer of heat between the atmosphere and the water are sparse. Experimental temperature profiles in water bodies exist, but the vertical resolution often does not allow for assessing small-scale turbulence effects or effectively investigating shallow variations of water temperature induced by the diurnal cycle of radiative forcing and air temperature. Also, profiles are usually constrained to the water body only and do not include near-surface air temperatures. Existing data sets of observed water temperature profiles are useful for their respective purpose but are inadequate for use in the present study, which aims at understanding the key processes that govern diurnal temperature evolution in superficial water layers. For instance, *Rodriguez-Rodriguez and Moreno-Ostos* [2006] have 10 thermistors between 0.5 and 2.5 m in the water and meteorological data at the shore, but not over the monitored water column. *Von Rohden et al.* [2007] measured high-resolution temperature profiles; however, the highest point is not above the epilimnion. Additionally, radiation and eddy diffusivity are crucial to determine, to properly simulate, and to predict the diurnal evolution of the temperature of a water column in still superficial waters such as lakes. Heat budget models for lakes can be found in the work of *Momii and Ito* [2008], *Babajimopoulos and Papadopoulos* [1986], and *McCormick and Scavia* [1981]; the required knowledge about the eddy diffusivity is, however, typically not available.

[1]School of Architecture, Civil and Environmental Engineering, Ecole Polytechnique Fédérale de Lausanne, Lausanne, Switzerland.
[2]Department of Civil and Environmental Engineering, Princeton University, Princeton, New Jersey, USA.
[3]Department of Biological and Ecological Engineering, Oregon State University, Corvallis, Oregon, USA.
[4]Institute of Geophysics, Université de Lausanne, Lausanne, Switzerland.
[5]Department of Physical Geography and Quaternary Geology, Stockholm University, Stockholm, Sweden.
[6]Bert Bolin Center for Climate Research, Stockholm University, Stockholm, Sweden.

0043-1397/11/2011WR010529

[4] During the lake-atmosphere turbulent exchanges experiment (LATEX) [*Vercauteren et al.*, 2009, 2008], a novel method was employed to measure the temperature profile below and above the water surface. Fiber optic-distributed temperature sensing (FO-DTS) allows measuring temperature with a resolution of 1 m along the fiber. In LATEX, the fiber was wrapped around a tube to obtain fine resolution measurements with an unprecedented spatial resolution of 3.78 mm and a time resolution of 5 min.

[5] The objective of this paper is to evaluate the potential of this measurement technique to estimate the effective thermal diffusivity of a water body. When daily temperature fluctuations are used to estimate the effective thermal diffusivity, transparency is an important factor in the propagation of heat into the medium [*Ohlmann and Siegel*, 2000; *Ohlmann et al.*, 2000; *Zaneveld et al.*, 1981], and must be appropriately considered in the analysis. A previous field study by *Neilson et al.* [2010] investigated the effect of solar radiation on FO-DTS in a river environment. Their findings suggest the presence of additional heating of the DTS due to solar radiation penetration at peak hours in aquatic environments. In the present paper, a simple model that describes heat propagation in a semitransparent medium is presented and is used to explain the temperature profiles observed during LATEX, and to assess the effects of water transparency on the apparent thermal diffusivity estimated by standard methods for opaque media.

2. Experimental Observations

[6] To date it has been difficult to obtain long time series of high-resolution vertical temperature profiles in water bodies by means of an automated, autonomous measurement system. Measurements close to the water surface are particularly difficult due to the presence of waves and periodical or episodic variations of the water level, which represent problematic conditions for data acquisition. Conventional measurement techniques usually consist of an array of thermistors or thermocouples configured at a selected vertical spacing. The resulting spatial resolution is usually too coarse to closely observe thermodynamic processes at the water surface or the temperature evolution in a shallow portion of the water where the diurnal cycle penetrates.

[7] In this study, fiber optic-distributed temperature sensing is used for the first time to obtain high-resolution measurements of water and near-surface air and water temperatures across the interface. DTS has recently been used in several environmental monitoring and research applications [*Roth et al.*, 2010; *Sayde et al.*, 2010; *Selker et al.*, 2006a; *Tyler et al.*, 2008, 2009; *Vogt et al.*, 2010; *Westhoff et al.*, 2007]. In summary, temperature can be measured along an optical fiber of several kilometers length with a spatial resolution of up to 1 m. The accuracy depends on the temporal resolution and increases for longer integration times, and decreases with the distance from the light source along the fiber. Typically, for a sampling frequency between 5 and 10 min, the accuracy is better than 0.1°C. Detailed information on the physical principle of DTS, which is based on Raman light scattering, is given by *Selker et al.* [2006b].

[8] To obtain a high-resolution temperature profile near the water surface, a 0.9 mm outer diameter gel-filled flexible cable containing an optical fiber was helically wrapped around a thin-walled 75 mm diameter PVC tube. The 754 m long fiber-optic cable was wrapped around the PVC tube until 2.85 m of the tube were entirely covered. Given the 1 m resolution along the fiber, this corresponds to 754 data points over the total tube length (including 3162 wraps of the fiber about the pole), and translates to an average spatial resolution along the pipe of 3.78 mm (Figure 1). The resulting sensor tube was painted white with antifouling marine paint to minimize the absorption of solar radiation during the daytime, and maintain a constant surface color.

[9] The sensor tube was vertically installed aside of a fixed platform located about 100 m offshore from the northern edge of Lake Geneva, near the village of Buchillon [*Vercauteren et al.*, 2008], in a shallow part of the lake of ~4 m depth without significant aquatic vegetation (only a few small pillows of algae were close to the bottom). Initially, ~1 m of the tube was above the water level, whereas the remaining 1.85 m extended into the water (Figure 1). The sensor tube was fixed with braces only at the top and bottom ends of the pipe to guarantee that the fiber-wrapped portion of the submersed tube section was completely in direct contact with the water. An array of five white plastic disks of ~40 cm diameter vertically spaced at 20 cm was

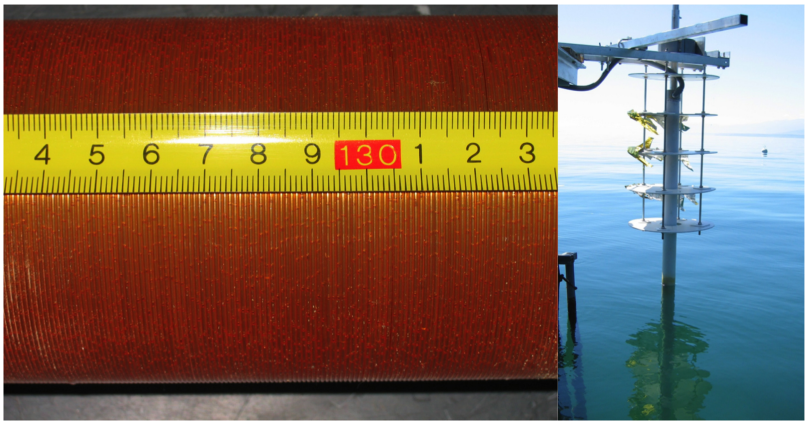

Figure 1. Close-up view of a section of the fiber wrapped sensor tube before painting (left) and sensor tube with radiation shield installed in the water (right).

installed around the tube section above the water level to minimize the effect of direct solar radiation on the sensor tube (Figure 1).

[10] Temperature data were taken using an Agilent Technologies N4386A DTS system during the LATEX field campaign from 15 August through 27 October 2006. Because of technical issues, two gaps of 8 and 3 d exist. The sampling frequency was 1 h, i.e., 24 profiles per day.

[11] Complementary measurements were taken on or near the platform. In particular, net radiation (Kipp and Zonen NR-Lite) as well as wind speed and direction (from a propeller anemometer and wind vane, Young R.M. Wind Monitor, and four 3-D sonic anemometers, Campbell Scientific CSAT3), were monitored during the field campaign.

3. Theory of Radiative Heating in Semitransparent Media

[12] To analyze the experimentally obtained water temperature profiles, we rely on the hypothesis that the main mechanisms affecting the diurnal temperature cycles close to the surface are the solar radiation forcing and the heat conduction enhanced by turbulent mixing. Here we assume that other factors contributing to the evolution of the vertical temperature profile are negligible. In particular, we neglect the effects of horizontal advection of water due to lake currents by assuming that the temperature and velocity profiles in the lake are horizontally homogeneous. This assumption is motivated by three practical and theoretical considerations.

[13] First, close to the lake surface the usual hypothesis that vertical gradients of temperature are larger than horizontal gradients holds, supporting the choice of considering primarily the vertical dynamics. Second, we apply our analysis only to the 24-h component of the temperature signal spectrum. As we expect that lake circulation dynamics are in general characterized by different temporal scales, this component is dominated by solar radiation forcing, which has a clear 24-h periodicity, and the working hypothesis that radiation and turbulent diffusivities are the key mechanisms is justified. Third, arising as an experimental constraint, the LATEX data set consists of one-dimensional, vertical measurements; therefore, it does not allow any consistent modeling of horizontal currents and the interpretative model has to be one-dimensional.

[14] Under the assumptions above, heat transfer close to the surface is governed by the following equation:

$$\frac{\partial}{\partial t}T = \frac{\partial}{\partial z}\left(D\frac{\partial}{\partial z}T\right) + \frac{H}{C}, \tag{1}$$

where T is the temperature (°C), C the volumetric heat capacity of the water (4.18×10^6 J/[°C m^3]), D the thermal diffusivity, which is dominated by eddy diffusion (m^2 s^{-1}), H the source term because of the local transformation of radiation into sensible heat in the water (W m^{-3}), and z is the vertical distance relative to the water surface.

[15] When radiation travels through the water, its intensity at a given wavelength decreases exponentially according to the Lambert-Beer's law [*Jerlov*, 1976]. The attenuation coefficient is strongly dependent on the wavelength: infrared radiation is absorbed within the first millimeters, whereas the shortest wavelengths can penetrate meters without significant attenuation [*Defant*, 1963; *Hale and Querry*, 1973]. As a consequence, the heat source term, H, has the form

$$H(z,t) = R(t)\sum_j \eta_j \mu_j e^{-\mu z}, \tag{2}$$

where the sum is taken over different components of the light spectrum; $R(t)$ is the total available radiation at the surface (W m^{-2}); η_j is the fraction of radiation at the surface due to j-th spectral component (-); and μ_j is absorption coefficient of the j-th spectral component (1 m^{-1}).

[16] Good approximations can be usually obtained by dividing the spectrum in only a few bands. *Rabl and Nielsen* [1975], for instance, have successfully used the five-band model presented in Table 1 (adapted from *Defant* [1963]). Absorption coefficients in Table 1 indicate that while short waves are poorly attenuated and long wave penetrate only few centimeters, absorption of intermediate wavelength radiation (0.6–1.2 μm) is important at a depth between 0 and 2 m, which approximately corresponds to the interval investigated in the LATEX experiment. The optical properties of natural water bodies also depend significantly on the water characteristics (turbidity, presence of organic matter, and vegetation), which can affect the absorption coefficient and the response at different wavelengths [see, e.g., *Kirk*, 1985].

[17] A simplified form for the incoming solar radiation at the surface is $\bar{R} + A_R\cos(\omega t)$, where $\bar{R}$ is the net solar radiation and A_R (W m^{-2}) the amplitude at the surface. Since we are interested only in diurnal temperature fluctuations (i.e., in the amplitude and phase shift of the 24-h component of the temperature signal), we can neglect the net solar radiation and assume that the incoming solar radiation at the surface is a simple harmonic function of time, i.e., $R(t) = A_R\cos(\omega t) = A_R\cos(2\pi t/\tau)$, where τ(s) is the period of oscillation. If we further assume that variations of D with the depth are negligible, we can readily solve equation (2) with the aid of complex numbers for a semi-infinite medium. We obtain the following vertical temperature profile

$$T(z,t) = A_0 e^{-kz}\cos(\omega t - kz + \phi_0) - \sum_j \gamma_j[e^{-\mu_j z}\cos(\omega t + \varphi_j) - e^{kz}\cos(\omega t + \varphi_j - kz)], \tag{3}$$

Table 1. Absorption Coefficients in Water and Radiation Fractions for Different Portions of the Solar Spectrum[a]

Portion of the Spectrum	I	II	III	IV	V
Light wave length (μm)	0.2–0.6	0.6–0.75	0.75–0.9	0.9–1.2	>1.2
Absorption coefficient, (μm^{-1})	0.032	0.450	3.000	35.00	258.0
Fraction of radiation, η(—)	0.237	0.193	0.167	0.179	0.224

[a]Data from *Rabl and Nielsen* [1975], as adapted from *Defant* [1961].

where we have defined

$$\gamma_j = \eta_j \mu_j \sin(\varphi_j) \frac{A_R}{\omega C}, \tag{4}$$

$$\tan(\varphi_j) = \frac{\omega}{D\mu_j^2}, \tag{5}$$

with $0 \leq \varphi_j \leq \pi/2$, and

$$k = \sqrt{\omega/2D} = \sqrt{\pi/\tau D}. \tag{6}$$

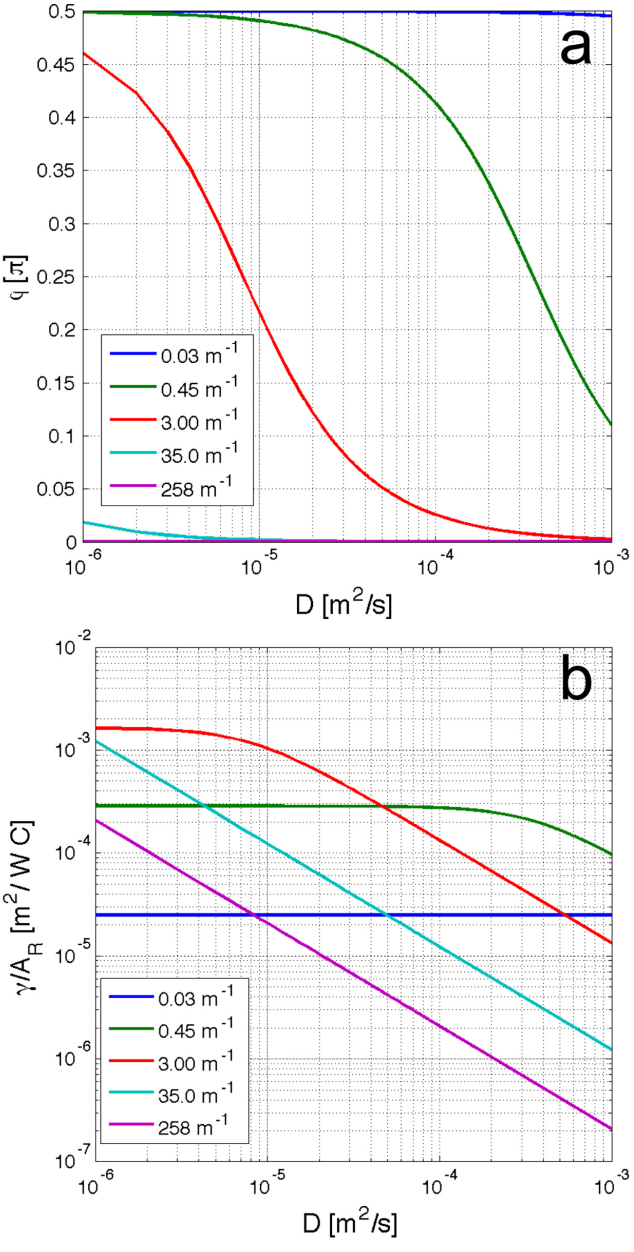

Figure 2. (a) Phase shift φ_j and (b) normalized surface amplitude of the radiative component γ_j as a function of the diffusivity for the different component of the solar radiation defined in Table 1. It is assumed that the radiation is a harmonic function of time with a period of 24 h.

[18] The coefficient A_0 (°C) is the amplitude of the diurnal temperature oscillation measured at depth $z = 0$ (e.g., close to the water surface), which has the form $T(z=0,t) = A_0 \cos(\omega t + \phi_0)$, where ϕ_0 is the time lag of the temperature oscillations with respect to the radiative forcing (temperature oscillations at the surface and radiation fluctuations are not necessarily in phase).

[19] The first term in equation (3) is the standard solution for the purely conductive problem [*Carslaw and Jaeger*, 1959], and shows that surface temperature oscillations are exponentially damped with depth, while maxima and minima are linearly delayed. Both exponential damping and linear phase shift depend on the frequency of the temperature signal and on the diffusivity D through equation (6). The summation term describes the effects of the radiative forcing. The first term in brackets is the heat source due to local absorption of radiation and transformation into heat;

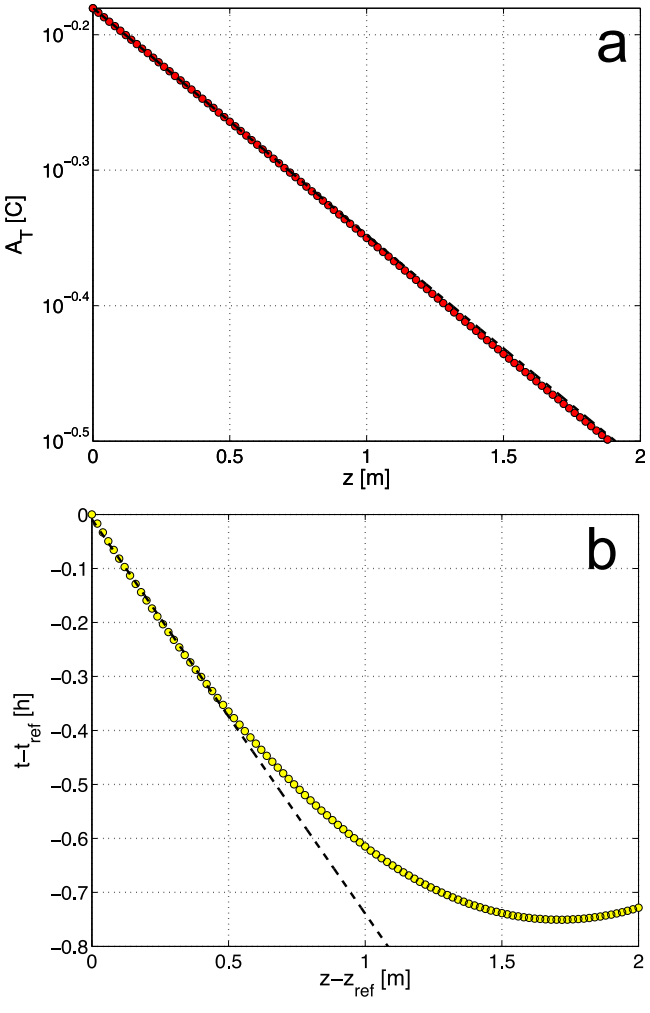

Figure 3. (a) Amplitude of the temperature fluctuation and (b) phase shift as a function of depth according to equation (3). The parameters used are: $D = 1.2 \times 10^{-4}$ m^2 s^{-1}; $A_0 = 0.66$°C; $A_R = 190$ W m^{-2}. The temperature maxima close to the surface are chosen to be lagged off 6.75 h with respect to the radiation maxima. Dashed lines are the exponential attenuation and linear phase shifts curved obtained by fitting the data only in the shallowest 0.5 m.

the second term is the conduction of the heat produced by this local source. Notice that the heat source also decreases exponentially with depth, but the phase shift is independent of the depth (see equation (5)). The dependencies of γ_j/A_R and φ_j on the diffusivity are plotted in Figure 2 for the different components of the solar radiation spectrum defined in Table 1, and for a forcing term with a period of 24 h.

[20] Assuming the five-band model in Table 1, the portions of the solar radiation spectrum that significantly contribute to the radiative term in the shallowest two meters are bands II (0.6–0.75 μm) and III (0.75–0.9 μm). Longer wavelengths are absorbed within the first centimeters and we assume that they will contribute only to the temperature fluctuations close to the surface (therefore, to the coefficient A_0); whereas absorption of shorter wavelengths can be neglected (Table 1). The half-temperature fluctuation, A_T, and the phase shift predicted by equation (3) are shown in Figure 3 as a function of depth. Here we assume a diffusivity $D = 1.2\ 10^{-4}$ m^2 s^{-1}, a surface amplitude of the temperature oscillation $A_0 = 0.66$°C (this corresponds to a 1.32°C difference between maxima and minima), and a total radiation amplitude of 190 W m^{-2} (380 W m^{-2} difference between maxima and minima, which is close to our measurements as we will illustrate in Figure 6). The lag parameter ϕ_0 in equation (3) is chosen such that the temperature close to the surface has maxima retarded of 6.75 h with respect to the radiation maxima. This time is derived from an observed lag in our data set.

[21] While temperature oscillation amplitude shows an attenuation that remains close to exponential, similar to the behavior of the purely conductive case, the radiative forcing has important qualitative effects on the phase shift. Indeed, at a certain depth, the phase shift ceases to be a linear function of depth (Figure 3). Quantitatively, however, the radiation influences the profile of both quantities.

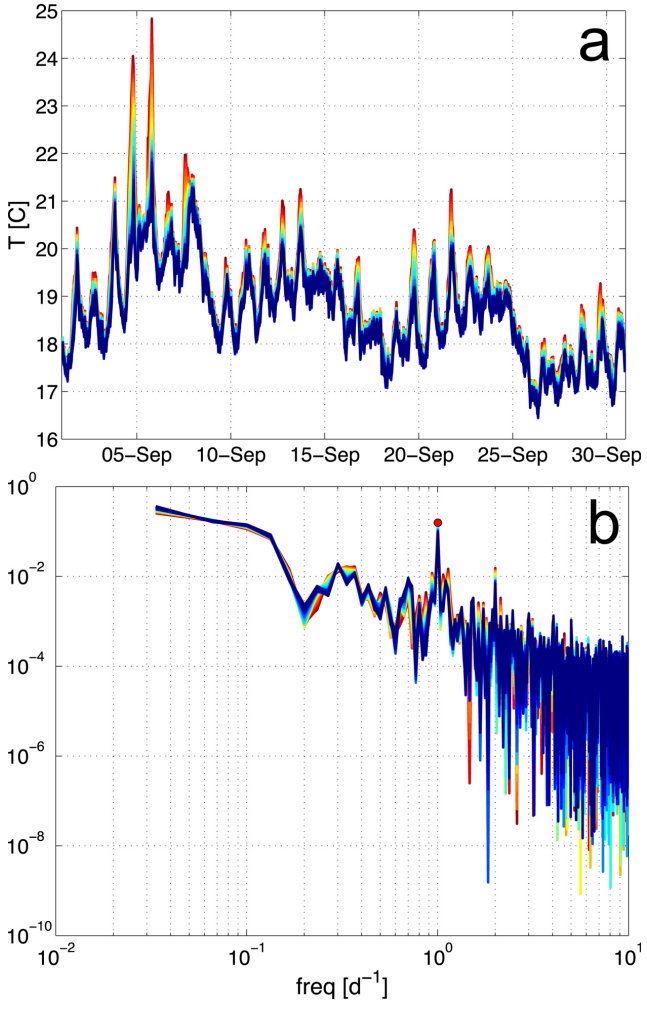

Figure 4. (a) Temperature evolution at different depths from 1 September to 1 October; shown are data recorded in the interval between 1.15 (red) and 2.75 m (blue) from the upper end of the sensor tube. (b) The power spectrum of the temperature time series at the respective depths.

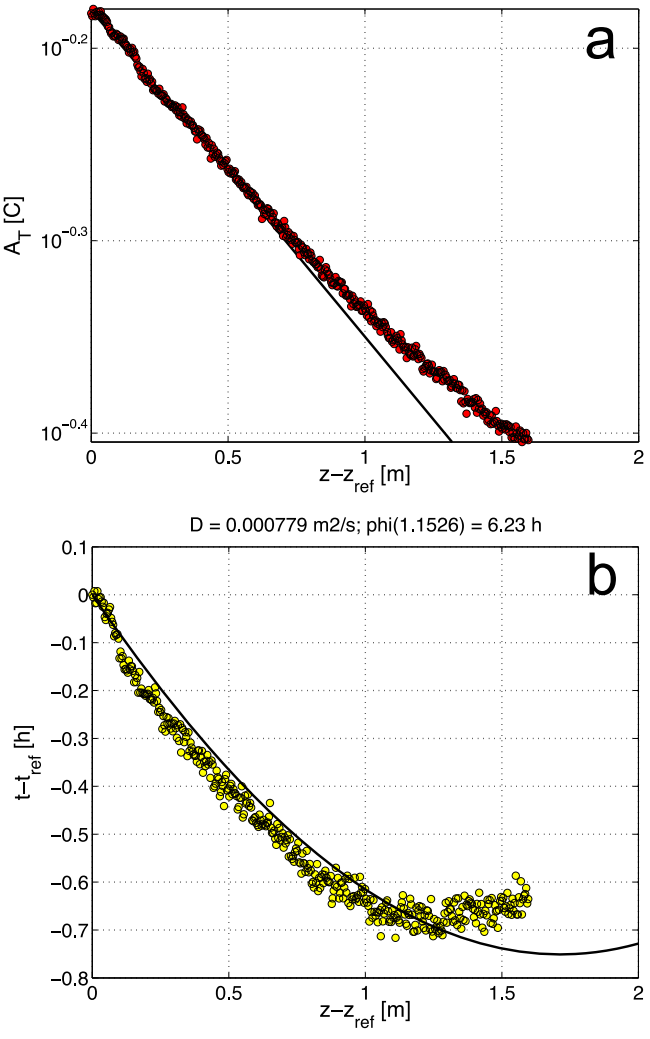

Figure 5. Analysis of the 1-d mode for the temperature between 1 September and 1 October (see Figure 3). (a) Amplitude of the daily temperature variation as a function of depth below the reference point; the diffusivity estimated from the slope of the data set in the first 0.5 m is $D = (2.41 \pm 0.04) \times 10^{-4}$ m^2 s^{-1}. (b) The phase shift as a function of the depth below the reference point; the estimated diffusivity is $D = (7.8 \pm 0.3) \times 10^{-4}$ m^2 s^{-1}. (In both plots the solid black lines reproduce the theoretical curves in Figure 2.)

Performing a standard Fourier analysis to estimate the diffusivity coefficient from the slopes of both curves in the first 0.5 m (where the amplitude attenuation profile is close to exponential while the phase-shift profile is close to linear) yields $D = (2.47 \pm 0.01) \times 10^{-4}$ m^2 s^{-1} from the analysis of the amplitude and $D = (10.05 \pm 0.05) \times 10^{-4}$ m^2 s^{-1} from the analysis of the phase shift. Both values are appreciably larger than the correct diffusivity used in equation (3), i.e., 1.2×10^{-4} m^2 s^{-1}. This shows that radiation can lead to an overestimation of the diffusive coefficient in transparent or semitransparent media, even in the presence of exponential attenuation and linear phase shift with depth, and that absorption must be explicitly considered to obtain reliable values of the effective thermal diffusivity. In this case, the discrepancy between the two estimates of the diffusivity can be used as an indicator showing that heat transport is not purely convective.

4. Data Analysis

[22] Temperature data were recorded from 15 August through 27 October 2006. The temperature evolution at different depths during the month of September is shown in Figure 4. Only the data in the interval between 1.15 and 2.75 m from the upper end of the sensor tube are presented, corresponding to data measured in the water body. The former point was estimated to be the shallowest point permanently below the water surface; the latter point was chosen because fiber termination effects, which cause oscillations in the signal, perturb observations close to the lower tube end. The temperature evolution clearly shows the influence of the diurnal cycle, dominated by the solar radiation forcing, as well as some longer timescales due to synoptic scale meteorological forcing and the seasonal trend.

[23] The importance of the diurnal cycle (i.e., the radiative forcing) is confirmed by the spectra of the temperature data, which exhibits a marked peak around a frequency of 1 d^{-1} (Figure 4). From the spectra, we isolate the 1-d mode and compute the amplitude and the phase shift associated with the diurnal temperature fluctuations. The vertical profile of the amplitudes below the water surface is shown in Figure 5, together with the phase shift, as a function of the distance from the reference point, $z_{\mathrm{ref}} = 1.15$ m. The amplitude of the temperature variation decreases almost exponentially in the water, as shown by the nearly straight line on a logarithmic scale. The phase shift, however, is more sensitive to the effects of radiation, and exhibits a minimum at a depth of about 1 m below the reference point. Applying the Fourier analysis to estimate the diffusivity based on the shallowest 0.5 m, one obtains $D = (2.41 \pm 0.04) \times 10^{-4}$ m^2 s^{-1} from the analysis of the amplitude and $D = (7.8 \pm 0.3) \times 10^{-4}$ m^2 s^{-1} from the analysis of the phase shift.

[24] In Figure 5, the theoretical curves (Figure 2) are also reproduced for comparison (solid black lines). In fact, these curves have been obtained using the maximum a priori information possible. For the solar radiation absorption we have used the five-band model suggested by *Rabl and Nielsen* [1975]. The amplitude of the near-surface temperature forcing has been obtained from the experimental data, i.e., $A_0 = 0.66$°C, whereas the lag between the temperature oscillation and the incoming radiation is chosen to be $\phi_0 = \tau/2\pi = -6.75$ h, which is close to the experimental value of -5.75 h. The amplitude of the total radiation forcing, i.e., $A_{\mathrm{R}} = 190$ W m^{-2}, corresponds to a maximum radiation of 380 W m^{-2}, which is close to the measured mean maximum net radiation (Figure 6).

[25] The quantitative agreement between experimental data and the theoretical curves is good, and confirms that a simple model based on the interplay between radiation absorption and eddy diffusivity is able to capture the main features of diurnal temperature evolution and to explain the experimental data. In particular, the nonlinear profile of the phase shift might be interpreted as a signature of the effects of radiation. The theoretical results of section 3 showed that performing a standard Fourier analysis of the amplitude decay or the phase shift overestimates the diffusivities even if the amplitude decay is close to exponential and the phase shift close to linear with the depth. In analogy with

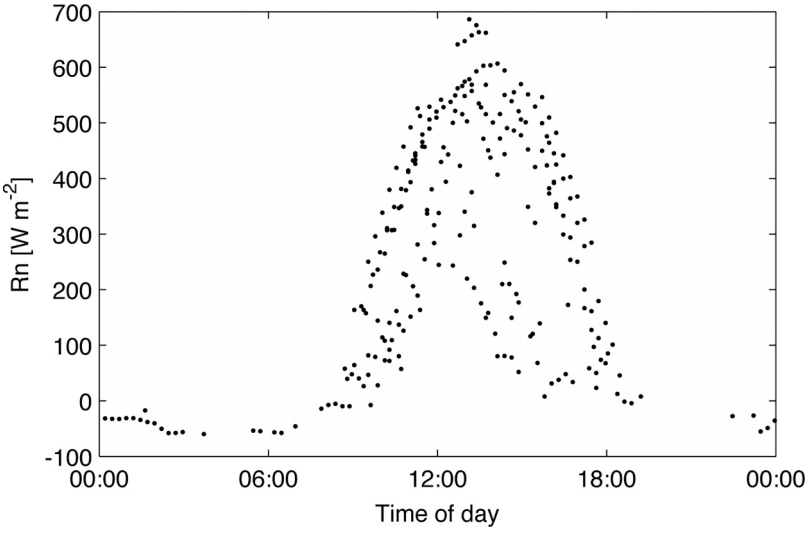

Figure 6. Diurnal variation of the net radiation during the period between 1 September and 1 October 2006. Each point represents a half-hourly averaged radiation measurement. The mean maximum net radiation is of the order of 400 W m^{-2}.

these results, we conclude that, because of the effect of the radiative forcing, Fourier analysis applied to the experimental data leads to an overestimated apparent thermal diffusivity even if it is applied in the first 0.5 m.

[26] Differences between the data and the theoretical curves are likely because of the specific optical properties of the lake, which depend on turbidity and the presence of organic matter [see e.g., *Kirk*, 1985], and might differ from the absorption model employed here (Table 1). Another factor possibly affecting the absorption coefficients is the effect of radiation absorption on the sensor tube, which absorbs some of the light that hits its surface, increasing the radiation effects with depth. *Neilson et al.* [2010] analyzed the warming of the fiber in an aquatic environment in more details and showed an exact quantification to be difficult. Our setup included several shielding disks around the tube that carried the fiber optic; however, these disks were limited to the portion of the fiber that was in the air, and radiative heating of the instrument was observed in this portion. Our data set did not enable us to further separate the effect of the radiation absorption by the sensor itself from the absorption by the water. It is clear that by varying the thermal diffusivity, the absorption coefficients, and the fractions of radiation, it is possible to improve the agreement between our model and the experimental data. As an example, Figure 7 shows the phase shift as a function of the depth obtained considering only a monochromatic radiation corresponding to band III (wavelengths 0.75–0.9 μm; $\eta = 0.167$) and varying the model parameters. A very good match between the data and theoretical curve can be obtained assuming $A_R = 190$ W m^{-2}, $\mu = 3.4$ m^{-1}, and $D = 0.8 \times 10^{-4}$ m^2 s^{-1}. It is also evident that a multiple band model allows perfectly matching all experimental data. However, we prefer not to engage in this fitting exercise. Without having measurements to constrain the model parameters, the risk is to employ an over-parameterized model that can describe any data set. For more quantitative analysis, more information is required particularly with respect to the optical properties of the water. Since these measurements are not available, we simply suggest that the good agreement between the experimental data and our simplified model with optical properties taken from the

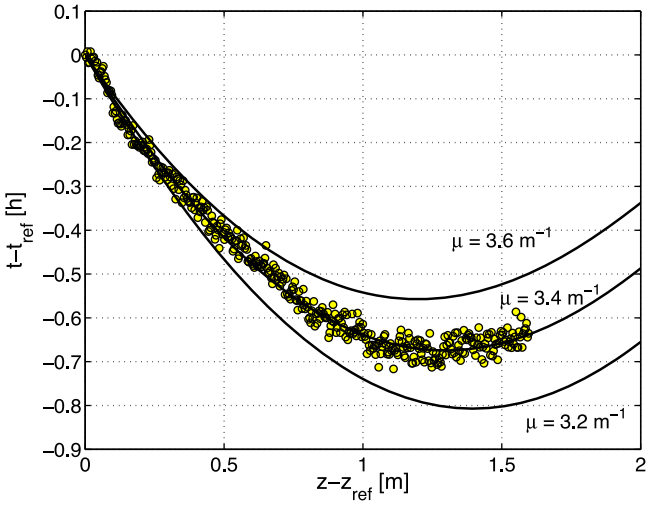

Figure 7. The p Phase shift as a function of the depth below the reference point. Circles represent the experimental data obtained from the analysis of the l-d mode for the temperature between 1 September and 1 October. Solid lines are obtained from equation (3) considering a monochromatic radiation corresponding to band III and varying the absorption coefficient. The other parameters used are: $D = 0.8 \times 10^{-4}$ m^2 s^{-1}; $A_0 = 0.66$°C; $A_R = 190$ W m^{-2}.

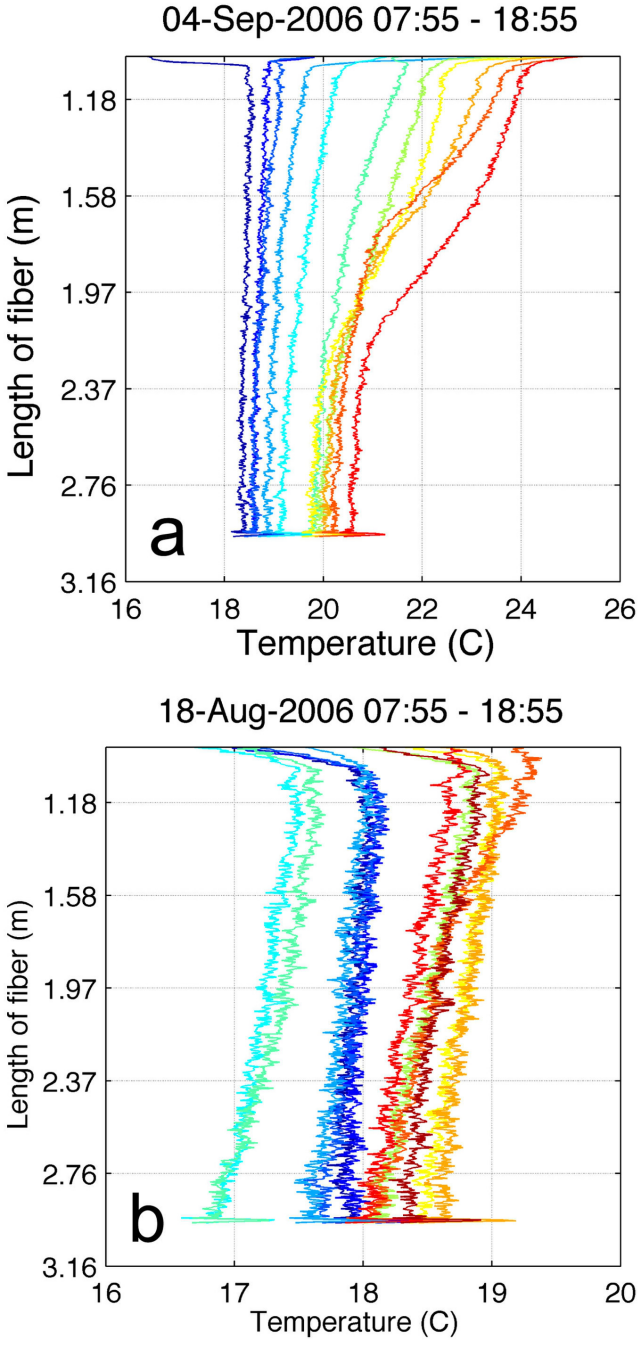

Figure 8. Evolution of temperature profiles (a) during a sunny day with low wind speed, 4 September, and (b) during a day with high wind speed, 18 August. Profiles are shown every hour from 8 a.m. to 7 p.m. (blue to red).

literature [*Rabl and Nielsen*, 1975] are an indication of the importance of radiative heating in the shallow water body. In the following we will focus on comparing the response of the system to variable wind and radiative forcings.

[27] To analyze in more detail how the interplay between conduction and radiation affects the water temperature profile, we focus on two days with very distinct meteorological conditions: a calm clear sky day, 4 September (Figure 8a), and a windy day, 18 August (Figure 8b). On a calm clear sky day, the effect of radiation clearly manifests in the important warming of near-surface water (Figure 8a). On the windy day, turbulent mixing is enhanced by the wind and the temperature changes are weak and homogeneous through the whole vertical profile (Figure 8b). The effect of radiative warming of the near-surface water is no longer apparent since locally heated water is effectively mixed. The two examples of temperature profiles during different meteorological conditions demonstrate that wind speed and solar radiation are crucial factors controlling the temperature profile close to the water surface.

[28] In the presence of strong wind the larger thermal diffusivity induced by turbulent mixing mitigates the effects of radiation; on the calm clear day, however, the radiative forcing can have a dominant effect on vertical temperature variations, and in particular on the phase shift. To investigate how different meteorological conditions impact the calculation of the thermal diffusivity, we perform a Fourier analysis on two periods of three days with very distinct characteristics.

[29] The first period, 4–7 September, is characterized by low maximum wind velocity (only 1.7 m s^{-1}) and by a mean net radiation of 166 W m^{-2}. Figure 9 shows the decay of the daily temperature amplitude and phase shift as a function of depth. The penetration and absorption of the radiation clearly yield a nonlinear phase shift. The diffusivities estimated from the slopes of the amplitude decay and

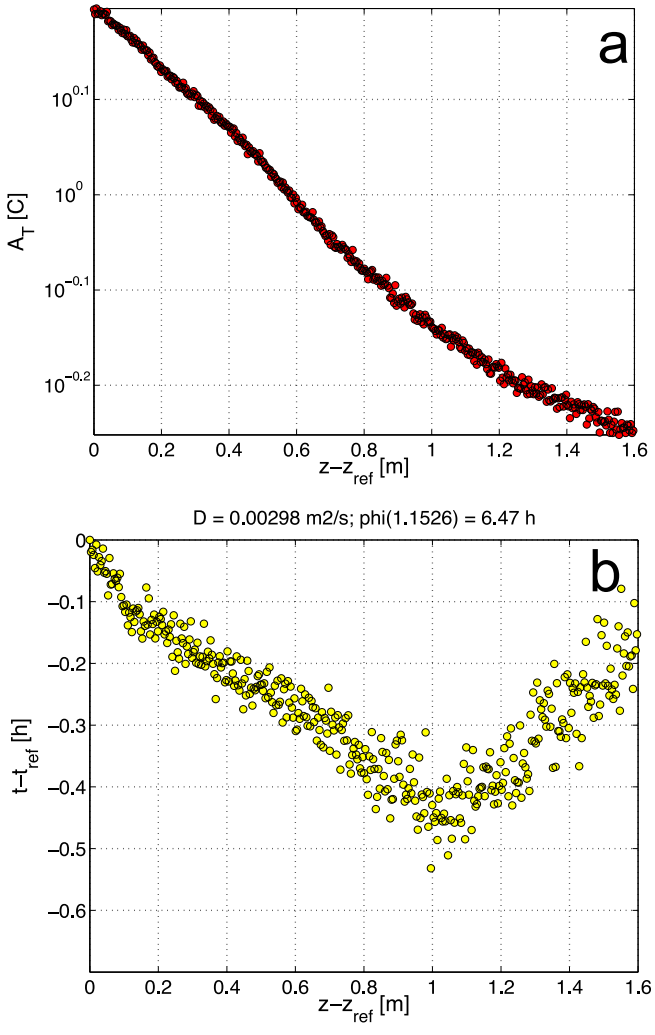

Figure 9. Analysis of the 1-d mode for the temperature from 4–7 September. (a) Amplitude of the daily temperature variation as a function of depth below the reference point; the diffusivity estimated from the slope of the data set in the first 0.5 m is $D = (6.6 \pm 0.1) \times 10^{-5}$ m^2 s^{-1}. (b) Phase shift with respect to the radiation as a function of the depth below the reference point; the estimated diffusivity is $D = (3.0 \pm 0.2) \times 10^{-3}$ m^2 s^{-1}.

of the phase shift in the first 0.5 m are $D = (6.6 \pm 0.1) \times 10^{-5}$ m^2 s^{-1} and $D = (3.0 \pm 0.2) \times 10^{-3}$, respectively. There is large disagreement between the two values because of the dominant effect of radiation that tends to drastically reduce the phase shift with depth, which results in a larger apparent diffusivity.

[30] During the second period, 15–18 August, the highest wind speed is 7.1 m s^{-1}, and the mean net radiation is 41 W m^{-2}. Figure 10 shows the decay of the daily temperature amplitude and the phase shift with depth. In this case, the phase shift is close to linear as a consequence of the dominant conductive effect, which reduces the impact of the radiation. The diffusivities estimated from the slope of the amplitude decay and the phase shift are $D = (9.1 \pm 0.4) \times 10^{-5}$ m^2 s^{-1} and $D = (2.6 \pm 0.2) \times 10^{-4}$ m^2 s^{-1}, respectively. The two estimated diffusivities are closer in this case, supporting the idea that the radiative forcing mainly induces differences in the estimates.

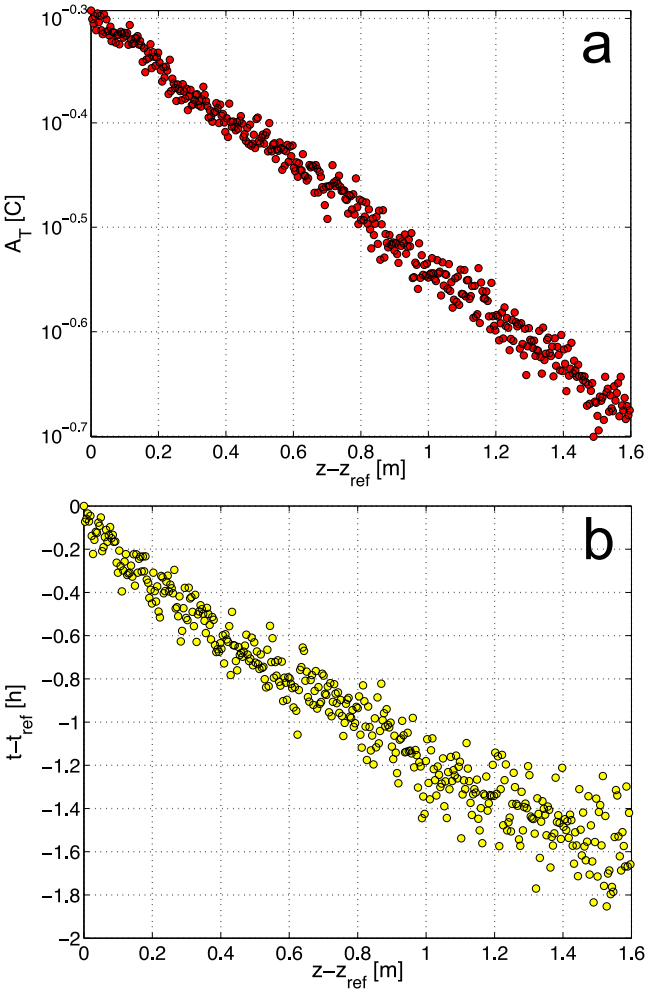

Figure 10. Analysis of the 1-d mode for the temperature from 15–18 August. (a) Amplitude of the daily temperature variation as a function of depth below the reference point; the diffusivity estimated from the slope of the data set in the first 0.5 m is $D = (9.1 \pm 0.4) \times 10^{-5}$ m^2 s^{-1}. (b) The phase shift with respect to the radiation as a function of the depth below the reference point; the estimated diffusivity is $D = (2.6 \pm 0.2) \times 10^{-4}$ m^2 s^{-1}.

5. Conclusions

[31] A new technique on the basis of the fiber optic distributed temperature sensing to measure high spatial resolution temperature profiles in and above a lentic water body is presented. Its ability to capture heat transfer from the atmosphere to the water body and vice versa is tested by the use of classical heat conduction analysis. The high spatial resolution (3.78 mm) permitted by the optical fiber allows detection of small temperature gradients, and enables observation of the effects of solar radiation on the temperature profile. The transfer of heat in the vertical direction from the atmosphere to the water is expected to follow a conductive process where the thermal diffusivity depends on turbulence in the water. The relative transparency of the media with respect to different wavelengths of incident light (solar radiation) is shown to affect the estimation of the thermal diffusivity from the temperature profiles. In particular, the linear phase shift of the diurnal temperature signal that can be observed in depth in the case of a conduction process is altered by the fraction of incident solar radiation transmitted directly into the water body. The main qualitative effect of the radiative forcing manifests in the slope of the phase-shift profile when the radiative contribution is important.

[32] Our analysis suggests that to obtain a correct estimate of the effective thermal diffusivity from a Fourier analysis, one needs a reliable estimation of the radiative term, which in turn requires complete knowledge of the optical properties of the lake water to avoid the problem of over-parameterization. A possible solution may be the measurement of radiation in the water; this would help in constraining the model by constraining the optical properties of the water. We remark that the good qualitative agreement between the experimental profiles of phase shift and oscillation amplitude and our model suggests that the latter captures well the involved key mechanisms.

[33] **Acknowledgments.** The authors acknowledge the technical help of Martin Tromp, and are grateful to EPFL for access granted to the Bois Chamblard areas for embarking. The project was funded by the Swiss National Science Foundation, grant nos. 200021_107910/1 and 200020_125092/1, NCCR Mobile Information and Communication Systems (MICS), and the Competence Center Environment and Sustainability (CCES): SwissEx. J. S. Selker was supported by the National Science Foundation grant no. 0711594.

References

Babajimopoulos, C., and F. Papadopoulos (1986), Mathematical prediction of thermal stratification of Lake Ostrovo (Vegoritis), Greece, *Water Resour. Res.*, *22*(11), 1590–1596, doi:10.1029/WR022i011p01590.

Brutsaert, W. (2005), *Hydrology: An Introduction*, vol. xi, 605 pp., Cambridge Univ. Press, Cambridge, New York.

Carslaw, H. S., and J. C. Jaeger (1959), Conduction of heat in solids, 2nd ed., 510 pp., Clarendon Press, Oxford, U.K.

Defant, A. (1963), Physical oceanography, *Annales De Geographie*, *72*(390), 195–196.

Hale, G. M., and M. R. Querry (1973), Optical-constants of water in 200-Nm to 200-Mum wavelength region, *Applied Optics*, *12*(3), 555–563.

Jerlov, N. G. (1976), *Marine Optics*, 246 pp., Elsevier Scientific Pub. Co., New York.

Katul, G. G., and M. B. Parlange (1992), A Penamn-Brutsaert model fro wet surface evaporation, *Water Resour. Res.*, *28*(1), 121–126, doi:10.1029/91WR02324.

Kirk, J. T. O. (1985), Effects of suspensoids (turbidity) on penetration of solar-radiation in aquatic ecosystems, *Hydrobiologia*, *125*, 195–208.

McCormick, M. J., and D. Scavia (1981), Calculation of vertical profiles of lake-averaged temperature and diffusivity in Lakes Ontario and Washington, *Water Resour. Res.*, *17*(2), 305–310, doi:10.1029/WR017i002p00305.

Momii, K., and Y. Ito (2008), Heat budget estimates for Lake Ikeda, *Japan, J. Hydrology*, *361*(3–4), 362–370.

Neilson, B. T., C. E. Hatch, H. Ban, and S. W. Tyler (2010), Solar radiative heating of fiber-optic cables used to monitor temperatures in water, *Water Resour. Res.*, *46*, W08540, doi:10.1029/2009WR008354.

Ohlmann, J. C., and D. A. Siegel (2000), Ocean radiant heating. Part II: Parameterizing solar radiation transmission through the upper ocean, *J. Phys. Oceanogr.*, *30*(8), 1849–1865.

Ohlmann, J. C., D. A. Siegel, and C. D. Mobley (2000), Ocean radiant heating. Part I: Optical influences, *J. Phys. Oceanogr.*, *30*(8), 1833–1848.

Penman, H. L. (1948), Natural evaporation from open water, *Proc. R. Soc. A*, *193*(1032), 120–145.

Priestley, C. H. B., and R. J. Taylor (1972), On the assessment of surface heat flux and evaporation using large-scale parameters, *Mon. Weather Rev.*, *100*(2), 81–92.

Rabl, A., and C. E. Nielsen (1975), Solar ponds for space heating, *Chemtech*, *5*(10), 608–616.

Rodriguez-Rodriguez, M., and E. Moreno-Ostos (2006), Heat budget, energy storage and hydrological regime in a coastal lagoon, *Limnologica*, *36*(4), 217–227.

Roth, T. R., M. C. Westhoff, H. Huwald, J. A. Huff, J. F. Rubin, G. Barrenetxea, M. Vetterli, A. Parriaux, J. S. Selker, and M. B. Parlange (2010), Stream temperature response to three riparian vegetation scenarios by use of a distributed temperature validated model, *Environ. Sci. Technol.*, *44*(6), 2072–2078.

Sayde, C., C. Gregory, M. Gil-Rodriguez, N. Tufillaro, S. Tyler, N. van de Giesen, M. English, R. Cuenca, and J. S. Selker (2010), Feasibility of soil moisture monitoring with heated fiber optics, *Water Resour. Res.*, *46*, W06201, doi:10.1029/2009WR007846.

Selker, J. S., N. van de Giesen, M. Westhoff, W. Luxemburg, and M. B. Parlange (2006a), Fiber optics opens window on stream dynamics, *Geophys. Res. Lett.*, *33*(24), L24401, doi:10.1029/2006GL027979.

Selker, J. S., L. Thevenaz, H. Huwald, A. Mallet, W. Luxemburg, N. V. de Giesen, M. Stejskal, J. Zeman, M. Westhoff, and M. B. Parlange (2006b), Distributed fiber-optic temperature sensing for hydrologic systems, *Water Resour. Res.*, *42*(12), W12202, doi:10.1029/2006WR005326.

Tyler, S. W., S. A. Burak, J. P. McNamara, A. Lamontagne, J. S. Selker, and J. Dozier (2008), Spatially distributed temperatures at the base of two mountain snowpacks measured with fiber-optic sensors, *J. Glaciol.*, *54*, 673–679.

Tyler, S. W., J. S. Selker, M. B. Hausner, C. E. Hatch, T. Torgersen, C. E. Thodal, and S. G. Schladow (2009), Environmental temperature sensing using Raman spectra DTS fiber-optic methods, *Water Resour. Res.*, *45*, W00D23, doi:10.1029/2008WR007052.

Vercauteren, N., E. Bou-Zeid, M. B. Parlange, U. Lemmin, H. Huwald, J. S. Selker, and C. Meneveau (2008), Subgrid-scale dynamics of water vapour, heat, and momentum over a lake, *Boundary-Layer Meteorol.*, *128*(2), 205–228, doi:10.1007/s10546-008-9287-9.

Vercauteren, N., E. Bou-Zeid, H. Huwald, M. B. Parlange, and W. Brutsaert (2009), Estimation of wet surface evaporation from sensible heat flux measurements, *Water Resour. Res.*, *45*, W06424, doi:10.1029/2008WR007544.

Vogt, T., P. Schneider, L. Hahn-Woernle, and O. A. Cirpka (2010), Estimation of seepage rates in a losing stream by means of fiber-optic high-resolution vertical temperature profiling, *J. Hydrology*, *380*(1–2), 154–164.

von Rohden, C., K. Wunderle, and J. Ilmberger (2007), Parameterisation of the vertical transport in a small thermally stratified lake, *Aquatic Sci.*, *69*(1), 129–137.

Westhoff, M. C., H. H. G. Savenije, W. M. J. Luxemburg, G. S. Stelling, N. C. van de Giesen, J. S. Selker, L. Pfister, and S. Uhlenbrook (2007), A distributed stream temperature model using high resolution temperature observations, *Hydrol. Earth Syst. Sci.*, *11*(4), 1469–1480.

Zaneveld, J. R. V., J. C. Kitchen, and H. Pak (1981), The influence of optical water type on the heating rate of a constant depth mixed layer, *J. Geophys. Res.*, *86*(C7), 6426–6428, doi:10.1029/JC086iC07p06426.

E. Bou-Zeid, Department of Civil and Environmental Engineering, Princeton University, Princeton, NJ 08544, USA.

H. Huwald, U. Lemmin, and M. B. Parlange, School of Architecture, Civil and Environmental Engineering, Ecole Polytechnique Fédérale de Lausanne, station 2, Bat. GR, 1015 Lausanne, Switzerland. (hendrik.huwald@epfl.ch)

I. Lunati, Institute of Geophysics, Université de Laussanne, CH-1015 Lausanne, Switzerland.

J. S. Selker, Department of Biological and Ecological Engineering, Oregon State University, Corvallis, OR 97331, USA.

N. Vercauteren, Department of Physical Geography and Quaternary Geology, Stockholm University, SE-10691 Stockholm, Sweden.